Southern Ocean Water Mass method: A new statistical approach using microfossil radiolaria for paleoceanographic insights for the Southwest Pacific sector of the Southern Ocean

V. Lowe, G. Cortese, Matthieu Civel-Mazens, H. Bostock

Quaternary Science Reviews 346 (2024) 109054

Contents lists available at ScienceDirect

Quaternary Science Reviews

journal homepage: www.elsevier.com/locate/quascirev

Invited Paper

Southern Ocean Water Mass method: A new statistical approach using microfossil radiolaria for paleoceanographic insights for the Southwest Pacific sector of the Southern Ocean

V. Lowe [a,b,*], G. Cortese [c], M. Civel-Mazens [d], H. Bostock [a]

[a] School of the Environment, University of Queensland, Brisbane, QLD, Australia
[b] Université de Bordeaux, CNRS, EPHE, UMR 5805, EPOC, Pessac, France
[c] Surface Geoscience, GNS Science, Lower Hutt, New Zealand
[d] Univ Brest, CNRS, IRD, Ifremer, UMR 6539, LEMAR, Plouzané, France

ARTICLE INFO

Handling editor: A. Voelker

Keywords:
Radiolaria
Water masses
Paleoceanography
Southern ocean
SW pacific

ABSTRACT

Ocean circulation and the formation and upwelling of water masses in the Southern Ocean play a critical role in the exchange of heat and carbon with the atmosphere over glacial-interglacial cycles, but the history of the subsurface water masses is poorly understood. Radiolarians inhabit the water column from the surface to the bottom of the ocean, and their distribution is known to be associated with water masses. We use radiolarian abundance census data from the SO-RAD core top dataset to explore the relationship between radiolarian distribution and surface and subsurface water mass structure of the Southwest Pacific Sector of the Southern Ocean. The species distribution was first explored using non-Metric Multidimensional Scaling. Then Multivariate Regression Tree (MRT) analysis was used to understand the relationship between radiolarian distributions and parameters of water mass boundaries (using isopycnal depths) and upwelling (using nutrient data). We identified a series of indicator species associated with oceanographic zones which were used to develop the Southern Ocean Water Mass Index. The contribution of the Index Species Groups provided further information on water column structure and the relative influence of the various water masses. The index was then applied to the radiolarian assemblage data from 2 previously published cores, Y8 and Y9, from the Subantarctic Zone east of New Zealand. The results of the Southern Ocean Water Mass Method showed changes in water mass structure through the last glacial-interglacial cycle at both core sites. The results agree with other proxy data from the region. The SOWM Method provides a new tool for understanding the history of changes in the water mass structure and circulation in the Southern Ocean.

1. Introduction

Radiolarians are a diverse group of siliceous microzooplankton that inhabit the entire marine water column. Previous work has shown that radiolarian species distribution is strongly related to temperature (Boltovskoy and Correa, 2016), hydrological fronts (Abelmann and Gowing, 1997) and water masses (Cortese and Prebble, 2015; Zoccarato et al., 2016). In this study, we utilise radiolarian assemblages to improve our understanding of the surface and subsurface water masses in the Southwest Pacific Sector of the Southern Ocean (SO) over the last glacial-interglacial cycle using a newly developed statistical Southern Ocean Water Mass (SOWM) Method.

The use of radiolarian assemblages in ocean sediments for paleoenvironmental studies began in the 1970s during the CLIMAP Project. Radiolarian abundances in sediments were utilised by applying factor analysis and transfer functions for estimating paleo-sea surface temperatures (CLIMAP, 1981, 1976; Imbrie and Kipp, 1971). Numerous radiolarian-based surface and sub-surface temperature records throughout the global oceans have contributed valuable insight into climate processes over glacial-interglacial cycles (Abelmann et al., 1999; Civel-Mazens et al., 2021; Cortese and Prebble, 2015; Hernández-Almeida et al., 2017; Matsuzaki and Itaki, 2017). Observations on radiolarian distributions associated with tropical upwelling zones led to the development of radiolarian-based paleoproductivity proxies. The Upwelling Radiolarian Index (URI; Caulet et al., 1992; Jacot Des Combes et al., 2005; Jacot Des Combes and Abelmann, 2007; Lazarus et al.,

* Corresponding author. School of the Environment, University of Queensland, Brisbane, QLD, Australia.
E-mail address: info@vikkilowe.com (V. Lowe).

https://doi.org/10.1016/j.quascirev.2024.109054
Received 12 July 2024; Received in revised form 27 October 2024; Accepted 27 October 2024
Available online 13 November 2024

2006; Rogers and De Deckker, 2007) and the Thermocline-Surface Radiolarian Index (Jacot Des Combes et al., 1999; Lazarus et al., 2006), utilised ratios of species that were known to dwell in regions of upwelling and at sub-thermocline water depths to understand the dynamics of such oceanographic systems in the past. A similar approach was used for the Water Depth Ecology (WADE) Index, this time linking upwelling processes to surface water productivity and the flux of organic carbon between surface and deep water (Lazarus, 2005; Lazarus et al., 2006, 2008; Rogers and De Deckker, 2007). This index had the advantage of being applicable over a greater range of climatic regions, including the high-latitude polar oceans. However, despite the pioneering efforts of many scientists (e.g., Abelmann, 1992; Abelmann and Gowing, 1997), there is a limited understanding of radiolarian species water depth preferences, particularly in the SO, and this hindered the use and interpretation of the WADE index for this region (Boltovskoy et al., 2010; Lazarus, 2005).

Over the last five decades, the continuous collection of radiolarian census data from SO sediment coretop samples has led to the first circumpolar Southern Ocean RAdiolarian Dataset (SO-RAD; Lawler et al., 2021). Lowe et al. (2022) explored the distribution of radiolarian assemblages of the SO-RAD. They concluded that SO radiolarians display strong associations with oceanographic features such as hydrological fronts, upwelling, and, importantly, isopycnal depth. Along with latitudinal differences, there is clear evidence of longitudinal variations in radiolarian distribution, with distinct ecoregions in the Atlantic, Indian, and Southwest Pacific sectors of the SO. Thus, when using the SO-RAD for exploring radiolarian environmental associations, and applying them to paleo-records, Lowe et al. (2022) recommended constraining the analyses and interpretations to a single sector of the SO.

In this paper, we use a subset of the SO-RAD radiolarian dataset (Lawler et al., 2021) and previously published downcore radiolarian assemblage counts from 2 cores, Y8 (Lüer et al., 2009) and Y9 (Panitz et al., 2015) from the Southwest Pacific sector of the SO to test a range of statistical approaches and develop a novel method for exploring water mass changes over the last glacial-interglacial cycle. First, we use non-Metric Multidimensional Scaling (nMDS) to visualise changes in radiolarian assemblages over time and identify periods of different assemblage composition. We then apply a newly developed SOWM Index based on the core top ecoregion assemblages identified by Lowe et al. (2022) to explore the changes in Index Species groups down core, and estimate the overall shifts in oceanographic conditions over a glacial-interglacial cycle. The results of the SOWM Index for cores Y8 and Y9 are compared to the previous paleo-proxy findings on these cores and other paleoceanographic evidence from around the region. The results show that the SOWM method has the potential to provide additional information on the paleoceanographic circulation of the SO, and new insights into subsurface processes.

2. Regional setting

The complex oceanography of the Southwest Pacific Sector is largely attributed to the bathymetric features of the New Zealand region (Chiswell et al., 2015). To the south of New Zealand lies the Macquarie Ridge which rises from the ~4000 m deep abyssal plain to ~1500 m depth on average, reaching above sea level at Macquarie Island. It has several narrow and deep passages (~4000 m) that channel the eastward-flowing Antarctic Circumpolar Current (ACC) and its associated hydrological fronts (Fig. 1; Rintoul et al., 2014; Sokolov and Rintoul, 2007). Hydrological fronts are regions of steep gradients in environmental variables and current speed, and their long-term median position is commonly used in paleoceaography to undersatnd environmental and biological shifts. Once the ACC has navigated its path through the gaps in the Macquarie Ridge it is then deflected south around the Campbell Plateau, which extends southeast from the South Island of New Zealand, generally at < 1000 m depth, though it reaches down to ~2000 m in some regions. Well-defined, steep boundary slopes

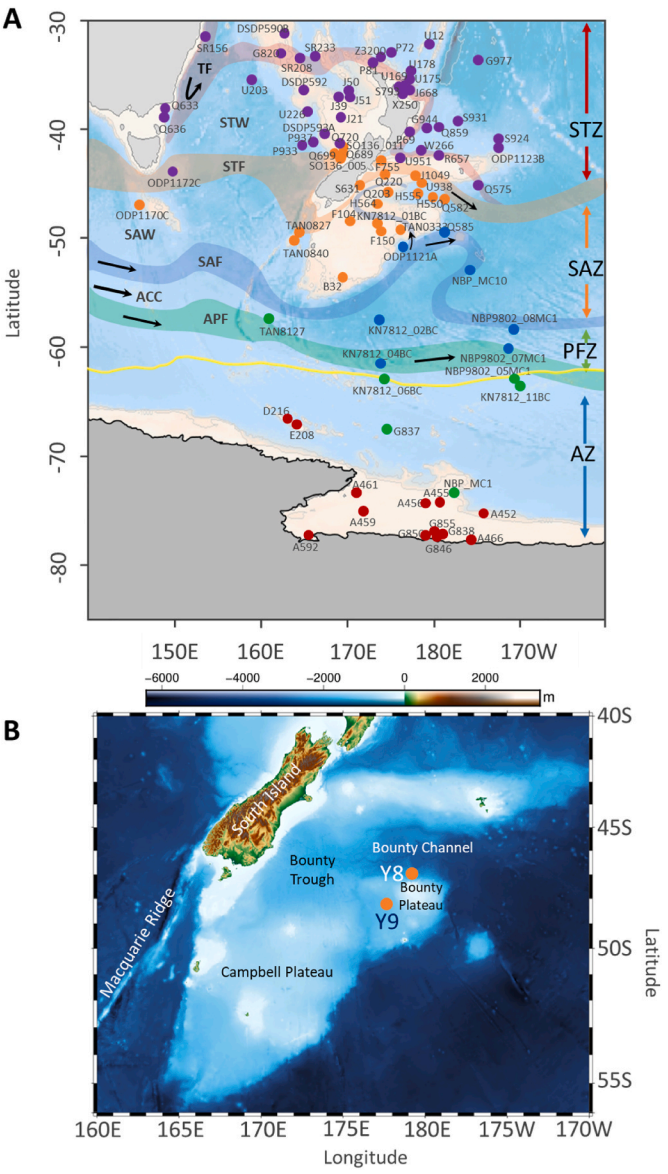

Fig. 1. A) Southwest Pacific sites of the SO-RAD core top dataset (Lawler et al., 2021). The distribution of sites within clusters identified by the MRT analysis for the Southwest Pacific Sector are identified by the colours of the sites. Zone A – red, Zone B – green, Zone C – blue, Zone D – orange, Zone E – purple. Main fronts and zones are shown STF; Subtropical Front – red band; SAZ, Subantarctic Zone; SAF, Subantarctic Front – orange band; PFZ, Antarctic Polar Frontal Zone; APF, Antarctic Polar Front – green band; AZ, Antarctic Zone (location of fronts and zones from Orsi et al., 1995; Bostock et al., 2013); Mean location of Winter sea ice margin (15%) – yellow line B) Bathymetric features of the Campbell Plateau and Chatham Rise region, and location of core sites Y8 (Lüer et al., 2009) and Y9 (Panitz et al., 2015). Modern zone of upwelling occurs south of the APF (Marshall and Speer, 2012).

separate the plateau from the abyssal plain of the South Pacific Basin (Heath, 1981). Overlying the Campbell Plateau is locally formed Subantarctic Mode Water (SAMW; Fig. 2; Forcén-Vázquez et al., 2021) and Subantarctic Surface Water (SAW; Bostock et al., 2013), while Antarctic Intermediate Water (AAIW) influences the plateau edges (Forcén-Vázquez et al., 2021). The Bounty Plateau, at the northeastern extent of the Campbell Plateau, is separated by the Pukaki Saddle, a 1250 m channel allowing Subantarctic Front (SAF) offshoots to enter the Bounty Trough, forming a cyclonic gyre (Neil et al., 2004). These offshoots of the SAF allow some mixing of the normally separated Circumpolar Surface Water (CSW) and SAW (Davis, 1998; Hayward

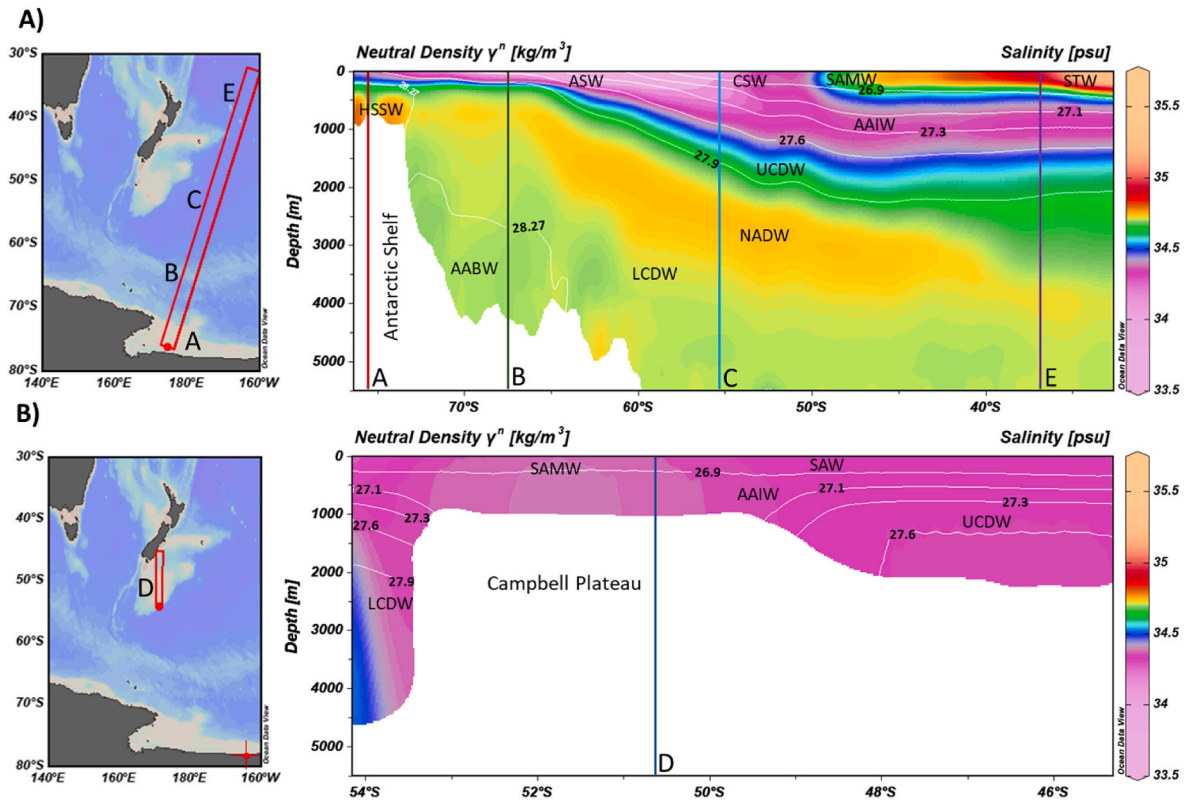

Fig. 2. *Transects of water column showing vertical water mass structure with salinity (colour) and neutral density (isolines) through A) the Open Ocean region of the Southwest Pacific Sector from 32°S to the Ross Sea Shelf 76°S, and B) the Campbell Plateau from 45°S to 55°S. ASW, Antarctic Surface Water; AABW, Antarctic Bottom Water; AAIW, Antarctic Intermediate Water; AASW, Antarctic Surface Water; CSW, Circumpolar Surface Water; HSSW, High Salinity Shelf Water; LCDW, Lower Circumpolar Deep Water; SAMW, Subantarctic Mode Water; SAW, Subantarctic Surface Water; STW, Subtropical Surface Water; UCDW, Upper Circumpolar Deep Water.* (Garcia et al., 2019).

et al., 2008). The Bounty Plateau acts as a barrier between the Bounty Trough to its north and the Pukaki Saddle to its south. Waters from the south influence the Pukaki Saddle, while the region north of the Bounty Plateau is influenced by eastward-flowing waters from the Bounty Trough, and water transported by eddy fields produced as the STF passes around the Chatham Rise's eastern end (Chiswell et al., 2015). The Bounty Trough deepens gradually eastward connecting with the deep South Pacific at the Bounty Fan (Carter et al., 2008). Within the Bounty Trough, Upper Circumpolar Deep Water (UCDW) is overlaid by AAIW and SAW, and some CSW due to the inflow from the Pukaki Saddle (Davis, 1998). The Subtropical Front (STF) flows around the southern tip of the South Island, then north along the shelf edge as the Southland Current (Sutton, 2003), continuing east along the southern flanks of the Chatham Rise. The STF is a shallow front where cool, macronutrient-rich Subantarctic Surface Water (SAW) interact with warm, salty, macronutrient-poor Subtropical Surface Water (STW). Around the South Island of New Zealand, the STF is also influenced by local neritic waters flowing in from rivers (Chiswell et al., 2015).

To the south and east of the Campbell Plateau lies the South Pacific basin, with abyssal plains extending to the Ross Sea Shelf. Here, Antarctic Bottom Water (AABW) is overlain by Lower and Upper Circumpolar Deep Water (CDW) and Antarctic Surface Water (AASW; Pellichero et al., 2018). In the Antarctic Zone, south of the Antarctic Polar Front (APF), westerly winds drive the Antarctic Convergence Zone, where CDW upwells. The lighter portion (<27.9 γ) flows north via Ekman transport, transforming into Antarctic Intermediate Water (AAIW) or Subantarctic Mode Water, while the heavier portion (>27.9 γ) moves south toward the Antarctic Shelf (Pellichero et al., 2018). Just north of the Ross Sea Shelf, cyclonic circulation forms the Ross Gyre. The gyre is dominated by CDW drawn from the ACC, and some of this CDW is transported onto the large embayment that forms the Ross Sea Shelf ranging in depth from ~200 to 1000 m (Locarnini, 1994). On the Ross Sea Shelf, Modified CDW (mCDW) and High Salinity Shelf Water (HSSW) are overlain by AASW. A large polynya in the Ross Sea produces large amounts of seasonal sea ice annually, producing HSSW, which flows down the slope and forms Ross Sea AABW (Orsi and Wiederwohl, 2009). Winter Sea Ice (WSI) in the Southwest Pacific sector of the SO extends as far north as 60–65°S (Crosta et al., 2022).

3. Southern Ocean Water Mass (SOWM) index development

3.1. SO-RAD core top assemblage data

Lowe et al. (2022) showed that radiolarian assemblages exhibit significant longitudinal heterogeneity in the SO, with clear ecoregions differentiated by basins and oceanographic conditions. Therefore, for this study, we have only included radiolarian assemblage relative abundance data from the Southwest Pacific region within the SO-RAD core tops (Lawler et al., 2021) from the Subtropics south of 30°S to the Antarctic coastline between 140°E to 170°W (Fig. 1A). The core top data is considered a modern representation of radiolarian assemblages as they appear in the surface sediments after sinking to the sea floor postmortem. We target the Southwest Pacific because the SO-RAD has better data coverage over the AZ compared to the other sectors. The dataset includes a total of 89 sites: 45 from the Subtropical Zone (STZ), 19 from the Subantarctic Zone (SAZ), 7 from the Polar Frontal Zone (PFZ) and 18 from the Antarctic Zone (AZ). While there is an imbalance in the number of samples from each zone, the techniques used for the

SOWM analyses (non-metric Multidimensional Scaling and Multivariate Regression Tree Analysis) do not weight their calculations based on this imbalance. Instead, they preserve the original dataset's characteristics and optimise their representation. Taxonomic categories within the SO-RAD data at the order level e.g. "Nassellaria Unknown" or "Spumellaria Unknown" were removed before the analyses in this study.

3.2. Environmental data

Climatological mean nutrient (nitrate, phosphate and silicate) concentrations at selected depth intervals, and isopycnal depth data (Table 1) were extracted from World Ocean Atlas (2018)1-degree grid (nutrient data) and 0.25-degree grid (density data) for Austral summer months when radiolarian abundances peak (JFM; Garcia et al., 2019). Extraction was performed in Ocean Data View v5.4.0 (Schlitzer, 2020). The chosen neutral density isopycnals represent specific water mass boundaries (Table 1).

3.3. Non-metric multidimensional scaling

The dissimilarity between species assemblages can be calculated using a distance matrix that contains values representing how similar (low values) or dissimilar (high values) the assemblages are between sites. Non-metric multidimensional scaling attempts to find the optimal representation of the dissimilarities within the distance matrix on a given number of axes. The stress value, between 0 and 1, indicates how well the nMDS plot represents the dissimilarity matrix, with lower values indicating better representation than higher values (Legendre and Legendre, 2012). Hellinger distance was calculated for SO-RAD (Southwest Pacific) relative abundance species data, and multidimensional scaling was performed for two dimensions (k = 2) using R Package *'vegan'* (Oksanen et al., 2019). The two nMDS axes were plotted using R Package *'ggplot2'* (Fig. 3; Wickham, 2016) to visualise dissimilarity between each site and explore gradients in the modern assemblage composition based on the major oceanographic regimes and water mass stucture in the Southwest Pacific Sector.

The nMDS plot (Stress = 0.112; Fig. 3) revealed that variability in radiolarian assemblages occurs along a gradient that represents a north-south trend from the STZ to the open ocean north of the Winter Sea Ice (WSI) margin (Fig. 1).

Sites within the STZ (purple circles) plotted separately from all other sites except for five core top sites. These five core top sites all occur in shallow shelf regions close to the coast and proximal to the STF, and instead plot with other shelf and plateau sites (orange) on the nMDS, close to the STZ sites. The variability in assemblage composition is higher for sites located in the open ocean south of the SAF to the Ross Shelf Slope (triangles and squares; blue, green and red) compared to the Campbell Plateau group (orange) and the STZ group (purple). The lowest variability was seen within the group of sites on the Ross Sea Shelf (red squares), which plotted as a distinct group.

Table 1
List of environmental variables used for analyses. For nutrient data, the numbers indicate the depth interval the measurement relates to. For isopycnals, the number refers to the density of the isopycnal. N, nitrate; P, phosphate; Si, silicate; AABW, Antarctic Bottom Water; AAIW, Antarctic Intermediate Water; LCDW, Lower Circumpolar Deep Water; SAMW, Subantarctic Mode Water; UCDW, Upper Circumpolar Deep Water.

Nitrate	Phosphate	Silicate	Isopycnal depth (m)	Isopycnal Water mass boundary
N_10	P_10	Si_10	Depth_26.9	AAIW/SAMW
N_100	P_100	Si_100	Depth_27.1	Mean AAIW
N_200	P_200	Si_200	Depth_27.3	UCDW/AAIW
N_300	P_300	Si_300	Depth_27.6	Upper/Lower Cells
N_400	P_400	Si_400	Depth_27.9	LCDW/UCDW
N_500	P_500	Si_500	Depth_28.27	AABW/LCDW

3.4. Redundancy and Multivariate Regression Tree analyses

Redundancy analysis (RDA) seeks to find the relationship between independent and dependent variables, in this case, species data and environmental variables. It performs a multivariate regression to understand how each environmental variable correlates with the species data. It then uses principal component analysis to lower dimensionality of the data for ease of interpreting the relationship between species and environmental parameters (Borcard et al., 2018). Hellinger, a square-root-based transformation, is commonly used in paleoecology to reduce the bias of highly variable relative abundance data, particularly where there are many zero counts. A RDA was performed on Hellinger transformed species data using each environmental variable individually to determine its explanatory power using R package *'vegan'* (Oksanen et al., 2019). The Lambda Ratio (λ_1/λ_2) was calculated for each variable by dividing the first constrained (RDA1, relating to the environmental variables) by the first unconstrained (PC1, relating to the species assemblages) eigenvalue (Juggins, 2013). In other words, if the Lambda Ratio is greater than 1, that parameter explains more species variability than not. Any variable with a Lambda Ratio below 1 was thus identified to have low explanatory power and eliminated from further analyses.

The isopycnal of 26.9 γ (Depth_26.9), representing the boundary between AAIW and SAMW (Table 1; Fig. 2), was determined to have low explanatory power (λ_1/λ_2) using RDA and Lamba ratio. It was, therefore, eliminated from further analyses. All remaining environmental variables were included in the MRT analysis.

Multivariate Regression Tree (MRT) analysis (De'Ath, 2002) is a constrained cluster analysis that highlights relationships between two datasets. The method uses recursive partitioning of one dataset (in this case, radiolarian species data) as it relates to categorical explanatory variables (in this case, isopycnal depths and nutrient concentrations, Borcard et al., 2018). The method produces a tree whose "leaves" represent clusters of sites that are defined by thresholds related to an explanatory variable. In this way, the clusters can be related back to the variables that define the cluster (Borcard et al., 2018). The MRT analysis was conducted using the R package *'mvpart'* (Therneau et al., 2022). In this study, MRT analysis was performed on Hellinger-transformed species data using Lambda-selected environmental variables to understand how the combination of environmental variables influences assemblage distribution. The MRT analysis was then performed using individual environmental variables to understand how each variable influences radiolarian distribution. Information about each cluster, the threshold for MRT-selected environmental variables that determine the cluster, cluster distribution and their indicator species, was then extracted from the results using the R package *'MVPARTwrap'* (Ouellette and Legendre, 2014).

The MRT analysis identified seven clusters that followed distinct water mass boundary regions, each representing a distinct water column structure. Two clusters were identified north of the STF, east and west of New Zealand. These two clusters were combined to represent the STZ jointly. A third cluster that consisted of a single site (J21) was identified in the STZ and was, therefore, not considered representative of an oceanographic region or condition. It was also included in the single STZ cluster. Four other clusters were identified south of the STF (Fig. 1). The distribution of the resulting 5 MRT clusters was similar to the variability shown by the nMDS plot (Fig. 3).

The indicator species identified by the MRT for each cluster formed the preliminary SOWM Index Species list, which included 74 of the 191 taxonomic units from the SO-RAD subset. A total of 26 species were eliminated due to their low indicator value (using a threshold value of <0.4, with 1 being highly representative, 0 not representative), 11 due to potential identification issues (e.g., easy misidentification between two species that represent different environmental conditions such as *Lithomelissa setosa* and *Trisulcus testudus*); 2 higher-level groupings that might contain multiple species that represent conflicting environmental

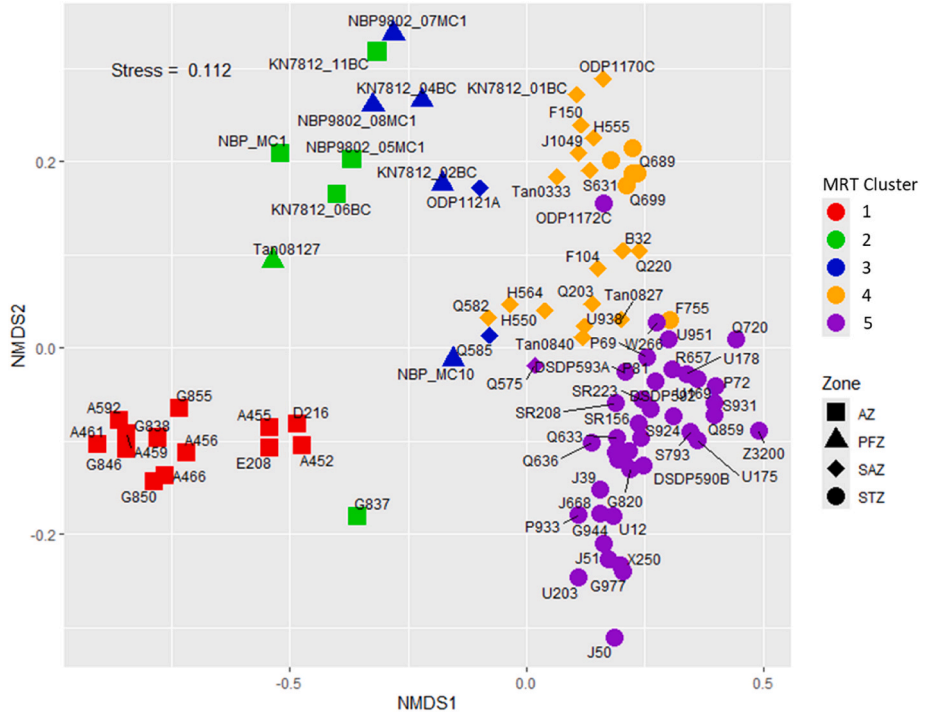

Fig. 3. Non-metric multidimensional scaling plot of Hellinger transformed radiolarian assemblage data for core tops south of 30°S in the Southwest Pacific Sector of the SO-RAD dataset. Colours represent the MRT clusters; shapes represent the latitudinal oceanographic zones. AZ, Antarctic Zone; PFZ, Polar Frontal Zone; SAZ, Subantarctic Zone; STZ, Subtropical Zone.

preferences were eliminated (e.g., *Lithomelissa* spp. and *Stylochlamydium* spp.). Two "spp." groups were included in the list, as they do not contain multiple unknown species or species that represent a range of conditions. *Carpocanistrum* spp. contains only STZ species and can be combined and utilised as a STZ signal. *Antarctissa* spp. include transitional forms between *A. denticulata* and *A. strelkovi*. The significance of these transitional forms is not fully understood. However, they were identified by the MRT analysis as an indicator group. A further 16 species were removed due to appearing in more than three clusters, or being absent from over 50% of sites within the cluster for which it was an indicator species. The final list for the SOWM Index contained 19 species (Table 2). From this point on, the species in the final list will be referred to as 'Index Species' for individual species, and 'Group' for all Index species within each MRT cluster and corresponding Index Zone.

3.5. Southern Ocean Water Mass Index development

The Index Species, categorised into five groups (A to E) as oulined in Table 2, were used to develop a SO water mass index (SOWM) for the Southwest Pacific sector. The SOWM is the ratio of the [Groups A:D sum + 1] divided by [Group E sum + 1]. The addition of '1′ to the sum of Groups A:D and the sum of Group E allows us to avoid any zero total for the numerator or denominator (which occurred at several sites in the SO-RAD). This ratio is summarised by the formula:

$$SOWM_{SWP} = \frac{\left(\sum_{A:D} S_{RA}\right) + 1}{\left(\sum_{E} S_{RA}\right) + 1} \qquad \text{(Equation 1)}$$

Where $SOWM_{SWP}$ is the index for the Southwest Pacific Sector of the SO, E = Group E, A:D = Groups A, B, C and D, S_{RA} = relative abundance of Index Species for clusters.

The rationale behind the index formula is that the abundances of Group E (5 species) decrease, while Groups A-D (14 species) increase south of the STF (Table 2). Equation (1) was applied to the Index Species of the Southwest Pacific SO-RAD core tops to validate its reconstructions of modern conditions (Table 2, Fig. 4A). The index value ranges showed a clear variation with specific oceanographic conditions, and corresponded well to the clusters determined by the MRT. A representative index value range and their threshold values were assigned to different oceanographic zones (Table 2). The Index Threshold Range refers to the range of values between each Index Zone, for which no SO-RAD core tops Index Values. Out of 89 sites, three outliers occurred, where their index values fell outside the range for their original MRT cluster assignment (Fig. 4A). Two sites (NBP9802-05MC1 and NBP9802-08MC1) are situated on the modern boundary between divergent upwelling and open ocean conditions. One site (H564) is located in the Bounty Trough in a region that regularly receives inflow from the SAF offshoot and is influenced by both shelf and open ocean conditions. The two adjacent oceanographic regimes likely influence each site over a decadal to centennial time scale (Sokolov and Rintoul, 2009). The nMDS plot also suggests that these sites are at the compositional boundary between two oceanographic settings (open ocean and upwelling or shelf and open ocean; Fig. 3).

The Index Species Groups total relative abundances (Index Species Relative Abundance, ISRA) were plotted for each SO-RAD site to show their influence on the final index value. The ISRA plot does not show the oceanographic regime itself, but rather the Index Groups proportions and, when applied down core, how these change through time (Fig. 4B and C). It is important to note that the association between the Index Species and their water masses is a statistical association, not deterministically known. The index zones are based on the RDA and MRT differentiation of assemblages, determined by water mass density boundaries throughout the water column (Table 1).

Table 2
List of Zones identified by the Index, the value ranges associated with each Zone, and the Index Species representative of those Zones. Threshold transition represents value ranges between the index values identified for each Zone. Please note that the Index Value Ranges refer to the results of the SOWM Index being applied to the SO-RAD assemblage data. These values do not refer to the Index Species or Groups.

Index Zone	Index Value Range	Threshold Range to Next Zone	Interpretation of Modern Distribution	Index Species within Groups
A	65–100	63–69	Seasonal Sea Ice Region	*Antarctissa denticulata* *Lithocampe furcaspiculata* *Lithocampe platycephala* *Lithomelissa* sp. *A* *Rhizoplegma boreale*
B	30–65	30–32	Upwelling of CDW	*Antarctissa strelkovi* *Artostrobus annulatus* *Cycladophora davisiana cornutoides* *Siphocampe arachnea* *Triceraspyris antarctica*
C	15–30	12–18	Open Ocean North of Upwelling	*Antarctissa* spp. *Cycladophora davisiana davisiana* *Saccospyris antarctica*
D	1–15	1	Temperate Shelf and Plateau	*Phorticium clevei*
E	0–1	–	Subtropical Region	*Amphirhopalum ypsilon* *Axoprunum stauraxonium* *Carpocanistrum* spp. *Didymocyrtis tetrathalamus* *Stylochlamydium asteriscus*

3.6. Summary of the Index Species Groups and their representations

- **Group A species** represent waters with a density higher than 27.9 γ, the boundary between UCDW and LCDW, and fated to be transported south toward the Antarctic Coast (Pellichero et al., 2018). Zone A, therefore, represents AABW and LCDW (or their associated properties, as with all the following water masses). It can also act as a guide for the Seasonal Sea Ice Zone, though with some limitations that will be discussed later.
- **Group B species** represent the lighter (27.6–27.9 γ) UCDW portion of upwelled water at the Antarctic Divergence Zone, which is moved northward by westerly winds and Ekman transport. This zone represents the addition of UCDW to the water column.
- **Group C species** represent the region where northward flowing waters transform and mix within the ACC and are fated to become Intermediate and Mode Waters, with a density range of 27.6–27.3. These waters are still at the surface and are not subducted, so this zone represents open ocean conditions between the upwelling zone and the SAF, where water properties are modified.
- **Group D species** represent the shallow region above the Campbell Plateau and shelf regions within the SAZ. This zone represents AAIW and SAW only, with a density range of 27.3 to 26.9 γ, as the shallow bathymetry excludes deeper water masses and their influences on radiolarian assemblages.
- **Group E species** represent the inclusion of Subtropical Surface Water (STW, <26.9 γ) and Pacific Deep Water (PDW) in the water column, and therefore waters sourced from the Subtropical region. This signal could be produced either by live specimens or the transportation of remains within a current moving from low or mid-latitudes to higher latitudes.

Here, it is important to note that 'upwelling' does not simply refer to the Antarctic Divergence Zone. It refers to any upwelling of deeper water masses to shallower depths. This includes mechanisms such as upwelling associated with topography or deep mixing.

3.7. Summary of SOWM method

The MRT analysis of the radiolarian census data provided clusters and their associated indicator species (Fig. 1). The relative abundances of the reduced indicator species (called the **Index Species**; Table 2) were then used to develop an index (Equation (1)). The index was applied to the radiolarian assemblage data for each Southwest Pacific site from the SO-RAD, and it was found that the sites from each of the 5 MRT clusters grouped together within 5 different value ranges between 0 and 100 (Fig. 4; Table 2). The value ranges relating to each cluster are classified as **Index Zones** (A to E; Table 2) which are associated with oceanographic regimes.

Application: The **SOWM Method** refers to the combined outputs, including the SOWM Index and the ISRA plots. The **SOWM Index** refers to the application of the index equation and the resulting index value that describes the overall oceanographic regime of the site. The **ISRA** refers to 1) the proportion of the **Index Species Groups** (A to E) within the total assemblage, and 2) the contribution of the Index Species Groups to the SOWM Index value, which provides a qualitative assessment of the subsurface water masses that are influencing the location. The SOWM Method in this study has been calibrated for the Southwest Pacific Sector of the Southern Ocean, and so should be applied to cores from this region only.

4. Application of the SOWM method downcore to assess paleoceanography

The SOWM Method was tested on previously published radiolarian assemblage counts from two Southwest Pacific cores, Y8 and Y9 (Lüer et al., 2009; Panitz et al., 2015). Core Y8 (1335 m water depth) is located within the SAZ, north of the Bounty Plateau and is influenced from the west by the Bounty Gyre outflow through the Bounty Channel (Fig. 2B). It is also influenced by eddies that are shed from the STF as the front passes around the eastern end of Chatham Rise (Lüer et al., 2009). Radiolarian assemblages were counted from 0 to 341 cm depth (52 samples), covering the last 265 kyr (Lüer et al., 2009). Core Y9 (1267 m water depth) is situated on the southwestern flanks of the Bounty Plateau in the Pukaki Saddle, near the SAF (Fig. 2B). It is predominantly influenced by southern-sourced water transported by offshoots of the SAF across the Pukaki Saddle (Panitz et al., 2015). Radiolarian assemblages were counted from 3 to 300 cm depth (61 samples), representing the last 163 kyr (Panitz et al., 2015).

The downcore radiolarian assemblages from Y8 and Y9 were analysed using 2-dimensional nMDS, and the results were plotted (Figs. 5

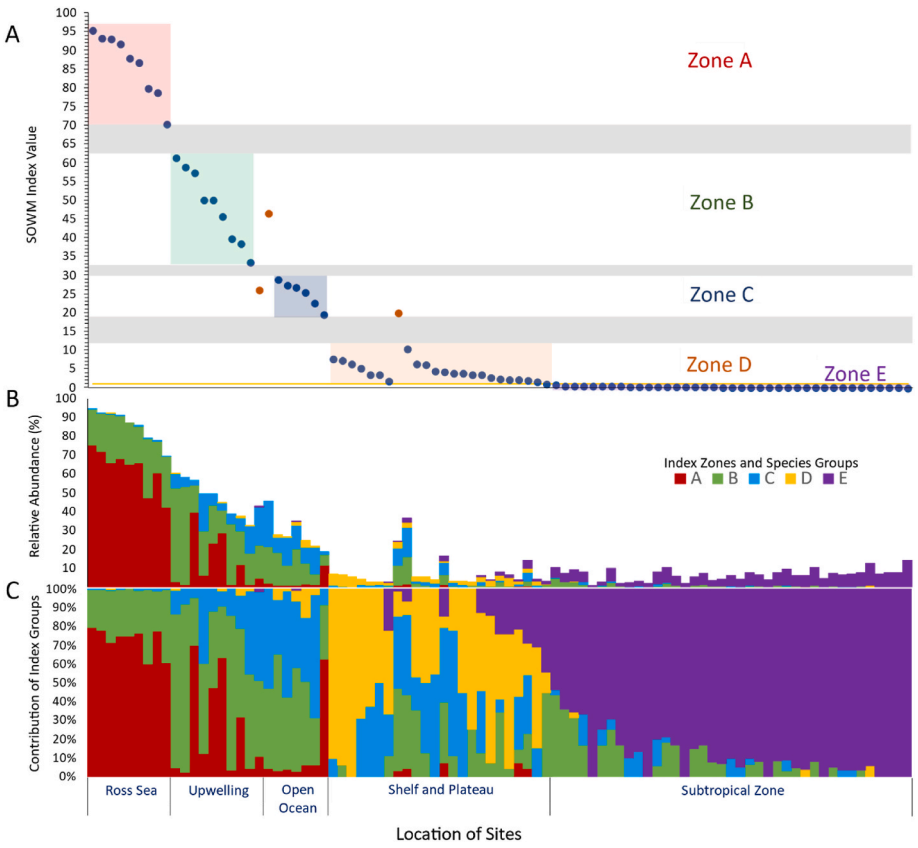

Fig. 4. A) SOWM Index values calculated using Index Species relative abundance data for each site south of 30° S within the Southwest Pacific Sector of the SORAD dataset. Sites are grouped according to the MRT cluster analysis determined using isopycnal and nutrient data. The major oceanographic features of each cluster are indicated on the x-axis. The grey-shaded areas represent the transition value ranges between zones. The yellow line is placed at the threshold value between Subtropical Zone (Zone E) sites and Shelf and Plateau (Zone D) sites. Orange data points represent outliers of the Index Zones B) Relative abundance plot of the total relative abundance of Groups within the whole assemblage. C) Index Species Relative Abundance (ISRA) plot showing the proportion of each Group at each of the SORAD sites.

and 7) to visualise the variability and dissimilarity of radiolarian assemblages through time within each core. The relative abundance data for the Index Species were extracted for each depth downcore to calculate the index value, as described earlier. The summed relative abundance for each Index Group (Table 2) was then plotted against age to show how each group contributed to the calculated index values. This ISRA plot (Figs. 5 and 7) visualises changes in the Index Groups through time.

4.1. Core Y8

The radiolarian assemblage data varied across marine isotope stages (MIS) 1–6, including distinctions between glacial periods (MIS 6 and 2), and between interglacials (MIS 5e and 1), as indicated by the distance between, and positioning of, the data points on the nMDS plot (Stress = 0.147; Fig. 5). The greatest variability occurred between interglacial assemblages and during transitional periods, from cold to warm (137.5–125.4 kyr; 21.7–10 kyr) and warm to cold (109.8–105.3 kyr). The spread of late MIS 1 data points may reflect sediment reworking in the uppermost 3 samples, as Neil et al. (2004) noted, so the variability shown by the nMDS plot is not interpreted here.

The results of the SOWM Index reveal that the site was dominated by three main oceanographic regimes over the study period. During glacial periods, the site fluctuated around the boundary between Zones C (open ocean) and B (upwelling). Peak interglacial periods exhibited Zone D (temperate shelf and plateau) conditions, followed by a shift back to Zone C around the start of MIS 5d and for the remainder of MIS 5 (Fig. 6A).

The ISRA plots (Fig. 6B and C) showed that Group B and C species were the dominant groups during peak glacial conditions. Peak interglacials showed a notable increase in Groups D and E, followed by an increase in Groups B and C during the remainder of MIS 5, returning to similar levels that were present during MIS 6 prior to the peak interglacial. Group E species disappeared at the end of MIS 5, but reappeared during MIS 3.

4.2. Core site Y9

Radiolarian assemblages during the two glacial periods of MIS 6 and MIS 3/2 show no overlap on the nMDS plot (Stress = 0.1479; Fig. 7). There is greater variability in assemblages during MIS 3 and 2 compared to MIS 6, although both glacials show less variability than interglacial periods. Some overlap was observed among interglacial assemblages. However, MIS 5e shows the greatest dissimilarity during peak conditions, while MIS 1 transitions away from assemblages present throughout the rest of the study period. The nMDS indicates that the assemblage at 120.25 kyr was notably distinct from the rest of MIS 5e, perhaps representing peak interglacial conditions.

The SOWM index results indicated that Zone B (upwelling) dominated at the site during the study period (Fig. 8A). During MIS 6, the

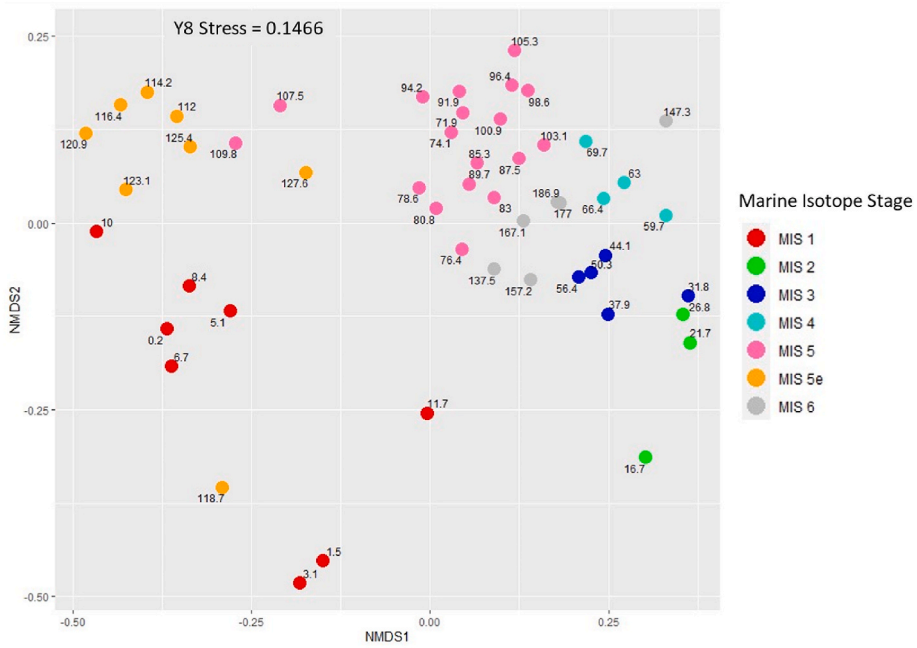

Fig. 5. Non-metric multidimensional scaling plot of Hellinger transformed radiolarian relative abundance data of core Y8. Colours are used to highlight each sample assignment to a Marine Isotope Stage (MIS) based on the samples age. Number labels associated with data points represent their approximate age (kyr; Lüer et al., 2009).

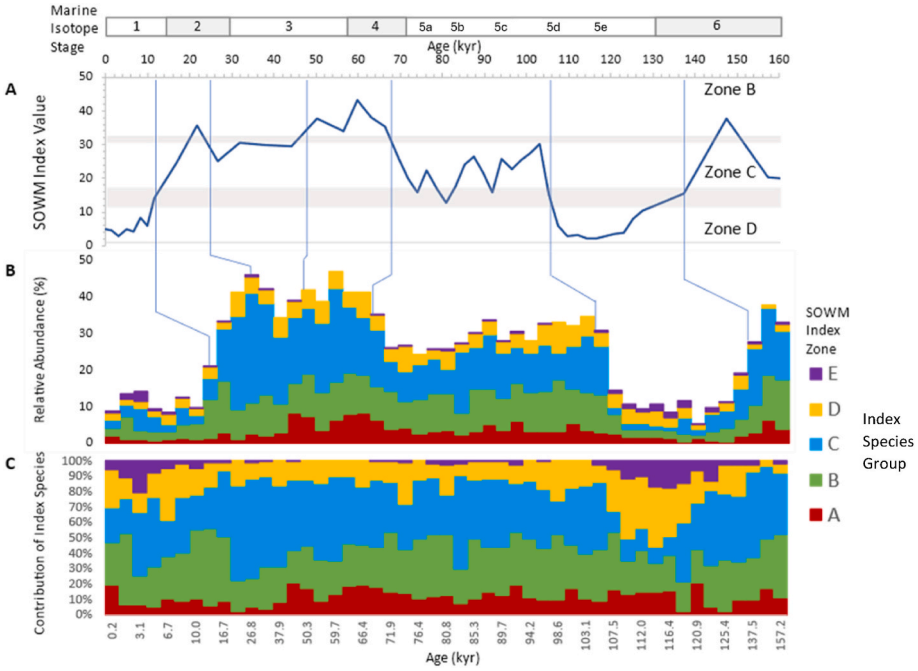

Fig. 6. Southern Ocean Water Mass (SOWM) plots for core Y8 of A) SOWM Index, B) relative abundances of Index Species within the whole assemblage, and C) stacked relative abundances of Index Species showing the proportion of each zonal group and their contribution to the SOWM Index values. Index Species are grouped and summed according to the Zone they represent (Zones A – E). Zone A – Seasonal sea ice zone, Zone B – upwelling zone, Zone C – open ocean, Zone D – Campbell Plateau, Bounty Trough and Shelf, Zone E – Subtropical Zone.

index values ranged from high Zone B to within the threshold between Zones A (Seasonal Sea Ice Zone) and B. These values were not reached during MIS 2. At both terminations into the interglacial periods, conditions changed to Zone D (temperate shelf). However, during MIS 5e, there was a transition back to Zone C (open ocean), which didn't occur during the Holocene.

The ISRA plots showed that Group C species dominated throughout the glacial periods, with Groups A and B also present, particularly at the

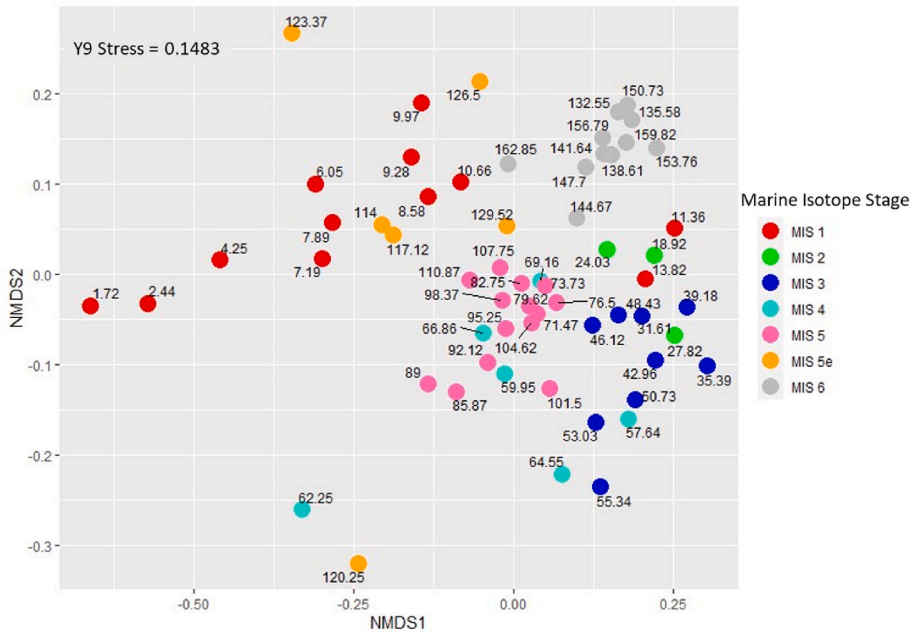

Fig. 7. *Non-metric multidimensional scaling plot of Hellinger transformed radiolarian relative abundance data of Core Y9. Colours are used to highlight each sample assignment to a Marine Isotope Stage (MIS) based on the samples age. Number labels associated with data points represent their approximate age (kyr; Panitz et al., 2015).*

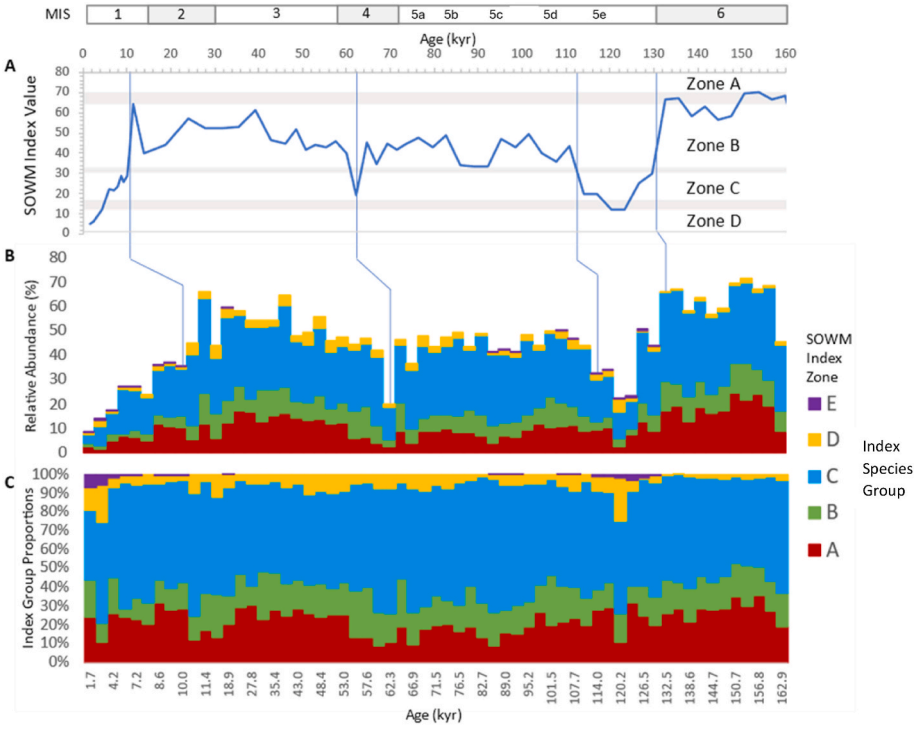

Fig. 8. Southern Ocean Water Mass (SOWM) plots for core Y9 of A) SOWM Index, B) absolute relative abundances of Index Species within the whole assemblage, C) stacked relative abundances of Index Species showing the proportion of each zonal group and their contribution to the SOWM Index values. Index Species are grouped and summed according to the Zone they represent (Zones A – E). Zone A – seasonal sea ice zone, Zone B – upwelling zone, Zone C – open ocean, Zone D – Campbell Plateau, Bounty Trough and Shelf, Zone E – Subtropical Zone.

glacial maximums. However, Group D and E species became more prominent in the assemblage during both peak Interglacials compared to glacial stages, when Group D species were much less abundant.

At both sites, the relative abundances of the Index Species were lower during peak interglacials, comprising around 10–20% of the assemblage compared to 30–40% at Y8 and 50–60% at Y9 during glacial periods. This decrease reflects an increase in species diversity during interglacial periods, including many species that did not meet the statistical criteria to be classified as Index Species groups.

5. Discussion

5.1. The SOWM method

While previous studies using radiolarian assemblages have focused on single environmental variables such as SST or subsurface temperatures, Lowe et al. (2022) demonstrated that the environmental drivers of radiolarian assemblages in the Southern Ocean (SO) are complex and vary between sectors. Based on the results of Lowe et al. (2022) and this study, it is evident that no single factor that influences the radiolarian species, but instead it is a combination of variables. Targeting water masses combines all these different variables, which affects the radiolarian community composition and abundance. We employed statistical techniques (nMDS, RDA, MRT) to establish a strong association between modern core top radiolarian assemblages and SO water masses.

Depth ranges of some radiolarian species vary widely in the literature (Boltovskoy and Correa, 2016). This variability may stem from sampling method differences, but the phenomenon of species occurrence deepening toward low latitudes compared to polar occurrences, attributed to isothermal submersion, is well-documented (Boltovskoy and Correa, 2016; Casey et al., 1982; Kling, 1976; Kling and Boltovskoy, 1995; Stepanjants et al., 2006). This was supported by previous studies that assessed the distribution and ecoregionalisation of the SO-RAD radiolarian assemblages (Lawler et al., 2021; Lowe et al., 2022). The ecoregions of modern Southwest Pacific radiolarian assemblages are separated by areas where changes in water mass structure occur (i.e., the addition of new water masses to the water column when moving north from the Antarctic Shelf to the STF; Lowe et al., 2022). This relationship allowed us to explore how radiolarian assemblages shift in conjunction with isopycnal outcropping (e.g., density changes related to water mass boundaries at regions of upwelling or water mass subduction) and the formation of water masses in the SO. The only region of water mass formation that was not significantly related to assemblage change in this study was the boundary between AAIW and SAMW. Applying the index to the cores in this study indicated that the current SOWM Index can provide valuable subsurface information for interpreting changes in water column structure over time.

The Index Zones have threshold ranges separating them, depicted in the Index plots as grey bands (Fig. 4, Table 2). These threshold ranges represent intervals where the SO-RAD dataset did not produce values when the Index was applied. Since these threshold values represent the boundary between two oceanographic regimes, they represent narrow geographical regions of rapid change, i.e., areas that lend themselves naturally to (under)sampling bias. The boundary between Zones D and E is well sampled, and so the threshold range is narrow. However, the other boundaries are undersampled in the SO-RAD, and so no analogues are currently available within these threshold ranges. As more core top data becomes available, it may better constrain the threshold ranges between zones.

The Index zones interpreted in the paper align closely with surface hydrological fronts, which are associated with water mass boundaries. Yet, caution is warranted when interpreting the Index as a tool for gauging surface frontal shifts. For example, Group E species may be related to Pacific Deep Water intrusion or the southward migration of warm-core eddies, both of which would produce a Zone E signal. Furthermore, water mass volume changes could occur without significant frontal shifts, and could result in a potential misinterpretation of the resulting index signal as north-south surface front migration. For example, the shoaling of UCDW that occurred during glacial periods (Elmore et al., 2015; Pahnke and Zahn, 2005; Ronge et al., 2015; Tapia et al., 2019) could mimic a modern divergent upwelling zone signal, and be misinterpreted as APF northward shift. Thus, caution is advised when using the methodology developed in the current study to interpret frontal shifts.

5.1.1. Seasonal sea ice

Zone A represents the region south of the 27.9 γ isopycnal boundary, and is associated with the lower cell of the meridional overturning circulation, which is driven by sea ice processes and freshwater fluxes (Pellichero et al., 2018). While Zone A indirectly suggests seasonal sea ice presence, it is not sufficient to confirm sea ice presence. In regions of the sea-ice zone where upwelling conditions are present, perhaps seasonally or forced topographically, Zone B values are produced. This occurred for sites on the eastern slopes of the Ross Shelf, where CDW is upwelled onto the shelf within the seasonal sea ice zone (Orsi and Wiederwohl, 2009), and on the Balleny Islands slopes, where an annual polynya forms (Ballard et al., 2010). The signal likely reflects the dominant conditions during peak summer conditions that impact radiolarian assemblages, when upwelling of CDW occurs and minimum sea ice is present. The strong relationship between radiolarian assemblages and seasonal sea ice, as identified by the nMDS plot (Fig. 3), suggests a separate Southern Ocean Sea Ice Index can be developed. This would assist in identifying the presence of seasonal sea ice at sites where mixed or transitional conditions exist within the upwelling and seasonal sea ice zones.

5.2. Paleoceanography of the Southwest Pacific sector using the SOWM method

The SOWM Method was applied to the radiolarian assemblages from two sedimentary cores from the Southwest Pacific, core Y8, north of the Campbell Plateau in the Bounty Trough, and core Y9 on the Pukaki Saddle (Figs. 1, 6 and 8). Both these sites are within the SAZ today (Fig. 1). The downcore results of the SOWM Method were compared to other paleoceanographic proxy data to assess this new paleo-water mass approach.

5.2.1. Glacials

The SOWM Index estimated the oceanographic regime at site Y8 during the glacial periods as open ocean conditions, with upwelling occurring at times (Fig. 6A). Site Y9 experienced upwelling for the majority of both glacial periods, and the influence of seasonal sea ice potentially extended/or ACC currents transporting associated radiolarian to the Pukaki Saddle during MIS 6 (Fig. 8A). Surface waters north and south of the Bounty Plateau were predominantly influenced by southern sourced CSW during both glacial periods (indicated by the increase in Zone C Index Species, Fig. 6B and C and Fig. 8B and C). The presence of southern sourced CSW was also indicated by radiolarian sea surface temperature (SST) estimates that placed Y9 surface waters between 1 and 2° colder during MIS 6 compared to MIS 2 (Panitz et al., 2015). Foraminiferal-based SST estimates from the Bounty Trough (DSDP Site 594) likewise show that MIS 6 was cooler than MIS 2 (Hayward et al., 2008). The presence of CSW in the region during glacial periods has been indicated based on a number of proxies including an increase in *Neogloboquadrina pachyderma* (ODP Site 1123, Crundwell et al., 2008; Hayward et al., 2008; Wilson et al., 2005), foraminiferal assemblage data (DSDP Site 594, Barrows et al., 2007), Mg/Ca derived SST from *Globigerina bulloides* (MD97-2120; Pahnke et al., 2003). Nannoplankton assemblage data (DSDP Site 594, Wells and Okada, 1997) also indicated that during the LGM the region was subject to cooler surface waters within the Bounty Trough. The presence of ice-rafted debris across the Campbell Plateau region, including at site Y9, indicates that water temperatures were cold enough to sustain the presence of ice at the ocean's surface (Carter et al., 2002). The cooler SSTs are thought to have been the result of a strengthened ACC and SAF and a northward shift of the APF, causing CSW to flow into the Bounty Trough via the Pukaki Saddle (Neil et al., 2004; Panitz et al., 2015).

During MIS 6, AAIW (Group D) was less prevalent compared to MIS 2 at the two sites, coinciding with increased open ocean conditions (Group C; Fig. 6B and C and Fig. 8B and C). Carbon isotope data from *Cibicidoides wuellerstorfi* at site MD97-2120 in the Bounty Trough

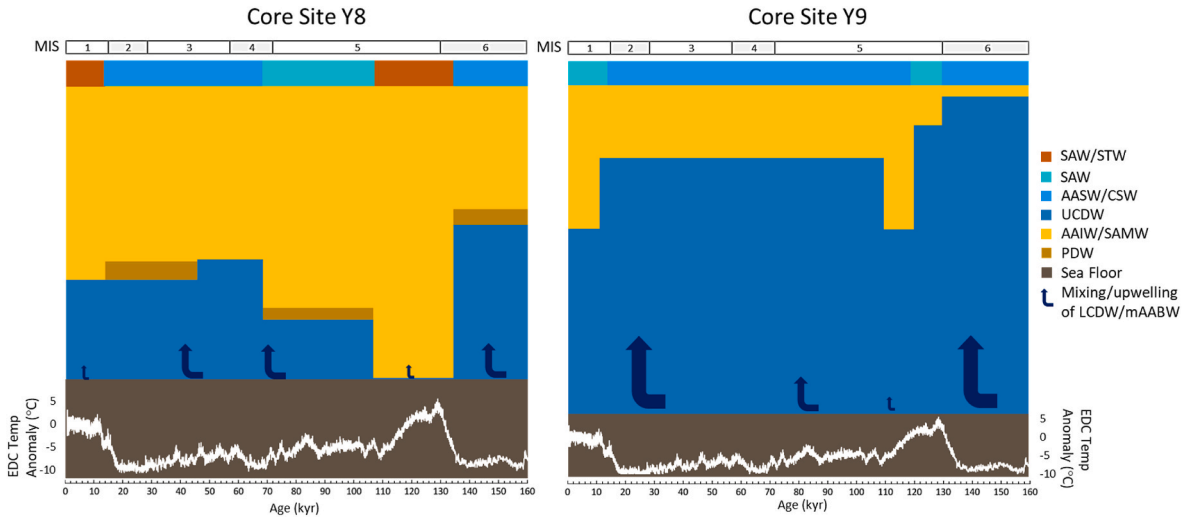

Fig. 9. *Schematic interpretation of relative water column structure changes based on the SOWM Index and relative contribution of index species (ISRA) at Core Sites A) Y8 and B) Y9 over the last glacial-interglacial cycle. The EPICA Dome C ice core temperature anomaly is overlaid on each graph showing the atmospheric temperature changes over the last 160 ky* (Lüthi et al., 2008) *SAW – Subantarctic Surface Water, STW – Subtropical Surface Water, CSW – Circumpolar Surface Water, AASW – Antarctic Surface Water, CDW – Circumpolar Deep Water, AAIW – Antarctic Intermediate Water, PDW – Pacific Deep Water, LCDW – Lower Circumpolar Deep Water, AABW – Antarctic Bottom Water, MIS – Marine Isotope Stage, size of blue arrow indicates interpreted strength of upwelling/vertical mixing of LCDW/AABW at the site.*

showed significantly decreased AAIW during MIS 6 compared to MIS 2, with indications of UCDW presence. This suggested greater shoaling of the AAIW/UCDW boundary during both glacials, particularly pronounced during MIS 6 (Ronge et al., 2015). Shoaling of this interface during glacial periods in the Southwest Pacific Sector has been further supported by Mg/Ca (a proxy for temperature), $\delta^{18}O$ (a proxy for salinity and temperature), and $\delta^{13}C$ (a proxy for water mass age) data from benthic and planktonic foraminifera (Elmore et al., 2015; Neil et al., 2004; Pahnke and Zahn, 2005; Ronge et al., 2015; Tapia et al., 2019). Tapia et al. (2019) noted stronger AAIW/UCDW shoaling and upwelling during MIS 6 compared to the LGM. During the LGM, ^{14}C data indicated slowed UCDW circulation and ventilation with younger and better-ventilated AAIW (Ronge et al., 2016; Sikes et al., 2000; Skinner et al., 2015).

The lower cell consisting of LCDW and AABW (Group A) reached its largest extent during glacial periods, particularly at site Y9, where it was most influential during MIS 6 (Fig. 6B and C and Fig. 8 B, C, Fig. 9). Benthic foraminiferal $\delta^{13}C$ data have indicated an increase in LCDW and Glacial Ross Sea Deep Water in the Southwest Pacific region during MIS 2, 4 and 6 (McCave et al., 2008). While the Southwest Pacific experienced increased lower cell influence during glacial times, McCave et al. (2008) concluded that MIS 2 experienced reduced LCDW contributions in the Bounty Trough region compared to MIS 4 and 6. This is supported by the decrease in group A indicating reduced LCDW influence at site Y8 during MIS 2.

As previously discussed, the upwelling signal may have overridden a seasonal sea ice zone signal at Y9 during glacial periods, particularly during MIS 6. The SOWM values (63–69) lie at the boundary between seasonal sea ice and upwelling zones (Fig. 8). The presence of seasonal sea ice cannot be conclusively determined by the SOWM during the penultimate glacial. However, it does suggest strong upwelling onto the Campbell Plateau at Y9. While the resolution of Y8 is lower than Y9, it appears that upwelling was also potentially present at Y8 during both glacials. Site Y8 does not show significant sea-ice assemblages during MIS 6 that resemble the sea-ice sites of the modern assemblages on the SO-RAD nMDS plot (Fig. 2). The MIS 6 assemblages at Y9 did show some separation from other periods, suggesting potential sea-ice influence during MIS 6 (Fig. 7).

Records for sea ice are absent between ~160°E and 170°W (Chadwick et al., 2022), making direct comparisons between previous records and the two cores in this study not possible. However, the SOWM method indicates that sea ice may have been present or influential in the region during MIS 6 and potentially MIS 2. SST records for the Tasman Sea and east of New Zealand indicate that minimum temperatures during the LGM could have been as low as 2 °C as far north as the Pukaki Saddle (Barrows et al., 2000). MIS 6 is thought to have been cooler than the LGM, based on foraminifera SSTs and assemblage data (Crundwell et al., 2008; Hayward et al., 2008; Panitz et al., 2015). Additionally, hydrological fronts were much further north during this period, and it is suggested that the SAF and ACC were compressed and intensified along the flanks of the Campbell Plateau (Neil et al., 2004; Wilson et al., 2005). There is also evidence for sea ice diatoms present in ODP 1123 north of the Chatham Rise, which are interpreted as being transported to the site via the ACC and the deep western boundary current (Stickley et al., 2004). This makes the presence of sea ice, or its influence on the microfossils, at the Pukaki Saddle conceivable. It is possible that a weak seasonal sea-ice zone signal, combined with a very strong upwelling signal (the potential scenario during MIS 6), could produce an index value that is higher than a combination of a weak seasonal sea-ice zone signal and moderate upwelling signal (the potential scenario during MIS 2).

The appearance of Group E (Subtropical Zone) species at the northern site during glacial periods suggests the influence of a northern-sourced water mass, interpreted here as Pacific Deep Water (PDW). This PDW could have carried a subtropical signal through the transport of radiolarian remains to the site. Some species from Group E, including *Amphirhopalum ypsilon, Didymocyrtis tetrathalamus* and *Stylochlamydium asteriscus*, have been recorded in plankton tows at depths over 500 m and down to 2000 m (Kling and Boltovskoy, 1995; Matsuzaki et al., 2020; Welling, 1997; Yamashita et al., 2002). The PDW signal appears to have reached the northern Bounty Plateau, but not the southern site, likely due to the fast-flowing SAF and ACC acting as barriers and preventing further incursion. Noble et al. (2013) used Nd isotopic data to suggest that PDW expanded its reach in the Southwest Pacific during the LGM. Ellwood et al. (2010) also indicated low ventilation and a southward expansion of PDW in the Pacific Sector of the SO, as suggested by higher concentrations of silicic acid. Radiocarbon analyses on benthic and pelagic foraminiferahave shown the presence of a very old (^{14}C-depleted) water mass south of the Chatham Rise during MIS3 and the LGM could again support the concept of a southward expansion of PDW in the region (Hayward et al., 2004; Pahnke and Zahn, 2005; Ronge et al., 2015, 2016; Anderson et al., 2024).

The Mernoo Saddle is the modern route of the STF and a region of cross-frontal transport. During the LGM, the STF is thought to have been located further north than its current position in the Tasman Sea and Campbell Plateau based on SST reconstructions (Barrows et al., 2000). A more northerly STF would have made the Mernoo Saddle a less likely transport path for Group E species. However, due to decadal variability of the fronts location and its transport of STW across Mernoo Saddle (Barrows et al., 2000; Chiswell et al., 2015), the possibility of an exchange across the Mernoo Saddle cannot be ruled out.

5.2.2. Glaciation – transition to a glacial maximum

There was a change in the oceanographic regime at Y8 from MIS 5e to MIS 5d (Fig. 6). During MIS 5d, open ocean conditions and UCDW influence (Zone B) markedly increased. This shift coincided with a change in the composition of benthic foraminiferal assemblages around the MIS 5e-d boundary (Hayward et al., 2004). Additionally, there was an increase in $\delta^{13}C$ of benthic foraminifera, and a decrease in $\delta^{18}O$ in planktic foraminifera within the Bounty Trough (Hayward et al., 2004; Pahnke and Zahn, 2005; Ronge et al., 2015).

The subtropical influence in surface waters decreased in this study region, as indicated by radiolarian-based SST estimates for both sites, which show a sharp decrease in temperature at the MIS5/4 boundary (Lüer et al., 2009; Panitz et al., 2015). At this time, conditions shifted to predominantly upwelling, and CDW influence increased, remaining strong through to MIS 2. While surface waters changed little thereafter, with similar SSTs from MIS 4 to 2 (Lüer et al., 2009), subsurface changes were evident, particularly the increasing influence of CDW from early MIS 4 to the LGM. At Y9, surface and subsurface conditions showed little change between MIS 5d and MIS 2. This site was predominantly influenced by CDW, though AAIW was also present, flowing onto the Campbell Plateau and over the Pukaki Saddle during this period.

5.2.3. Terminations and interglacials

At the two Terminations documented in the two downcore records (TI, MIS 2/1; TII, MIS 6/5e), the transition into interglacial conditions was similar. Y8 shifted from upwelling (Zone B) to shelf and plateau (Zone D) conditions, and then remained relatively steady throughout the interglacial period. Y9 also experienced this shift, but shorter peak interglacial conditions (Fig. 6A and 8A).

During both interglacials, the Bounty Trough (Y8) became flushed with AAIW and SAW, with a strong influence from the STZ (Fig. 6B and 9). This structure was more pronounced during MIS 5e than during MIS 1. Similarly, the Pukaki Saddle (Y9) experienced increased influence from AAIW, SAW, and STZ during both interglacials. However, being more exposed to the open SO, CDW influence persisted during interglacial, but to a lesser extent than during glacials (Fig. 8B and 9).

Multiple proxies have indicated the increased presence of SAW, AAIW, and input of STW in the Bounty Trough during interglacial periods. During MIS 5e, maximum foraminiferal-based SSTs were estimated to be ~4.7 °C higher than modern temperatures in the Bounty Trough, and ~3.5 °C higher on the Pukaki Saddle (Cortese et al., 2013). Dinoflagellate and foraminiferal assemblages at DSDP Site 594 indicated the presence of SAW and increased STF influence during the Holocene, likely due to enhanced eddy activity in the region (Prebble et al., 2017; Neil et al., 2004). Foraminiferal assemblage data indicated an increase in Southland Current sourced waters and potentially STW flowing southwards through the Mernoo Saddle into the Bounty Trough (Cortese et al., 2013). Foraminiferal stable isotope data indicated that the vertical extent of AAIW was greater during MIS 5e compared to MIS 1, with a deeper AAIW/UCDW boundary during the former. Consequently, the water masses below AAIW had less influence on the water column during both interglacials, particularly during MIS 5e (McCave et al., 2008).

6. Conclusion

The application of the newly developed SOWM Method to radiolarian assemblages in the Southwest Pacific sector of the SO has provided valuable new insights into oceanographic regime shifts and subsurface water mass changes over the last glacial-interglacial cycle. This study demonstrates that radiolarian communities are sensitive indicators of complex environmental dynamics, reflecting changes in water mass boundaries. By employing statistical techniques such as nMDS, RDA and MRT, we established robust associations between modern radiolarian assemblages and SO water masses, elucidating their responses to past climatic variations.

Applications of the new SOWM Method on two cores from the region shows that during glacial periods, the Bounty Plateau region featured cold surface waters sourced from the south, coupled with strong upwelling and an influx of CDW. Sea ice potentially influenced Y9 during MIS 6, while Y8 may have been influenced by northern-sourced PDW. Interglacial periods showed a subtropical influence on surface waters, likely due to a southward shift of the STF and increased eddy activity transporting subtropical waters south of the Chatham Rise. During these warmer time intervals, there was a greater presence of subsurface AAIW over the Campbell Plateau and Bounty Trough, along with a reduction in CDW.

The interpretations from the SOWM Method are consistent with previous paleoceanographic findings using isotopic and microfossil studies. The newly developed method thus represents a valuable new tool for paleoceanographers, offering a nuanced understanding of subsurface oceanographic changes in the SO over glacial-interglacial cycles.

CRediT authorship contribution statement

V. Lowe: Conceptualization, all analyses, method development and interpretations, writing of original draft, editing and writing of all subsequent drafts. **G. Cortese:** Conceptualization, assistance with method development, Validation, review and editing of all drafts, Supervision. **M. Civel-Mazens:** Assistance with methodology validation and interpretation of results, reviewing and editing of drafts. **H. Bostock:** Conceptualization, assistance with method development, Validation, review and editing of all drafts, Supervision.

Funding sources

VL was supported by an Australian Research Training Program (RTP) scholarship. VL and MMC visited Simon Fraser University, funded by MITACS with Globalink Research Award (IT28615). GC contribution was supported by the New Zealand Ministry of Business, Innovation and Employment through the Antarctic Science Platform (ANTA1801) and the Global Change through Time Programme (GCT SSIF, contract C05X1702).

Declaration of competing interest

The authors declare that they have no known competing financial interests or personal relationships that could have appeared to influence the work reported in this paper.

Acknowledgements

Thanks to Dr. Karen Kohfeld for her input in the testing and interpretation of the SOWM Method during the 3-month MITACS-funded collaboration at Simon Fraser University, British Columbia, Canada. Thanks to Dr. Kathy Gunn for her contributions to the interpretation and discussion section of this manuscript. Thanks also to all those who provided feedback at the ICP14 Poster Session, Bergen, Norway. Thank you to the reviewers who provided valuable comments which assisted in improving the manuscript for publication.

Data availability

Data will be made available on request.

References

Abelmann, A., 1992. Radiolarian taxa from Southern Ocean sediment traps (Atlantic sector). Polar Biol 12, 373–385. https://doi.org/10.1007/BF00243108.

Abelmann, A., Brathauer, U., Gersonde, R., Sieger, R., Zielinski, U., 1999. Radiolarian-based transfer function for the estimation of sea surface temperatures in the Southern Ocean (Atlantic sector). Paleoceanography 14, 410–421. https://doi.org/10.1029/1998PA900024.

Abelmann, A., Gowing, M.M., 1997. Spatial distribution pattern of living polycystine radiolarian taxa - baseline study for paleoenvironmental reconstructions in the Southern Ocean (Atlantic sector). Mar. Micropaleontol. 30, 3–28. https://doi.org/10.1016/S0377-8398(96)00021-7.

Anderson, H.J., Chase, Z., Bostock, H.C., Noble, T.L., Shuttleworth, R., Taiapa, B., Chen, W.H., Ren, H., Jacobsen, G.E., 2024. Millennial-scale carbon flux variability in the subantarctic pacific during marine isotope stage 3 (57–29 ka). Paleoceanogr. Paleoclimatol. 39. https://doi.org/10.1029/2023PA004776.

Ballard, G., Toniolo, V., Ainley, D.G., Parkinson, C.L., Arrigo, K.R., Trathan, P.N., 2010. Responding to climate change: adélie Penguins confront astronomical and ocean boundaries. Ecology 91, 2056–2069. https://doi.org/10.1890/09-0688.1.

Barrows, T., Juggins, S., De Deckker, P., Calvo, E., Pelejero, C., 2007. Long-term sea surface temperature and climate chnage in the Australian-New Zealand region. Paleoceanography 22 (2).

Barrows, T.T., Juggins, S., De Deckker, P., Thiede, J., Martinez, J.I., 2000. Sea-Surface temperatures of the Southwest Pacific ocean during the last glacial maximum. Paleoceanography 15, 95–109. https://doi.org/10.1029/1999PA900047.

Boltovskoy, D., Correa, N., 2016. Biogeography of radiolaria polycystina (protista) in the World Ocean. Prog. Oceanogr. 149, 82–105. https://doi.org/10.1016/j.pocean.2016.09.006.

Boltovskoy, D., Kling, S.A., Takahashi, K., Bjorklund, K.R., Bjørklund, K., 2010. World atlas of distribution of Recent Polycystina (Radiolaria). Palaeontol. Electron. 13, 1–229.

Borcard, D., Gillet, F., Legendre, P., 2018. Numerical Ecology with R, second ed. Springer International Publishing, Cham.

Bostock, H.C., Sutton, P.J., Williams, M.J.M., Opdyke, B.N., 2013. Reviewing the circulation and mixing of Antarctic Intermediate Water in the South Pacific using evidence from geochemical tracers and Argo float trajectories. Deep. Res. Part I Oceanogr. Res. Pap. 73, 84–98. https://doi.org/10.1016/j.dsr.2012.11.007.

Carter, L., McCave, I.N., Williams, M.J.M.M., 2008. Chapter 4 circulation and water masses of the Southern Ocean: a review. Dev. Earth Environ. Sci. 8, 85–114. https://doi.org/10.1016/S1571-9197(08)00004-9.

Carter, L., Neil, H.L., Northcote, L., 2002. Late quaternary ice-rafting events in the SW Pacific Ocean, off eastern New Zealand. Mar. Geol. 191, 19–35. https://doi.org/10.1016/S0025-3227(02)00509-1.

Casey, R.E., Spaw, J.M., Kunze, F.R., 1982. Polycystine radiolarian distributions and enhancements related to oceanographic conditions in a hypothetical ocean. Trans. Gulf Coast Assoc. Geol. Soc. 32, 319–332.

Caulet, J.P., Vénec-Peyré, M.T., Vergnaud-Grazzini, C., Nigrini, C., 1992. Variation of South Somalian upwelling during the last 160 ka: radiolarian and foraminifera records in core MD 85674. Geol. Soc. Spec. Publ. 64, 379–389. https://doi.org/10.1144/GSL.SP.1992.064.01.25.

Chadwick, M., Crosta, X., Esper, O., Thöle, L., Kohfeld, K.E., 2022. Compilation of Southern Ocean sea-ice records covering the last glacial-interglacial cycle (12-130ka). Clim. Past 18, 1815–1829. https://doi.org/10.5194/cp-18-1815-2022.

Chiswell, S.M., Bostock, H.C., Sutton, P.J.H., Williams, M.J., 2015. Physical oceanography of the deep seas around New Zealand: a review. New Zeal. J. Mar. Freshw. Res. 49, 286–317. https://doi.org/10.1080/00288330.2014.992918.

Civel-Mazens, M., Crosta, X., Cortese, G., Michel, E., Mazaud, A., Ther, O., Ikehara, M., Itaki, T., 2021. Antarctic polar front migrations in the kerguelen Plateau region, Southern Ocean, over the past 360 kyrs. Glob. Planet. Change 202, 103526. https://doi.org/10.1016/j.gloplacha.2021.103526.

CLIMAP, 1981. Seasonal reconstruction of the Earth's surface at the last glacial maximum. Geol. Soc. Am. Chart Seri. MC-36.

CLIMAP, 1976. The surface of the ice-age. Earth Sci. 191.

Cortese, G., Dunbar, G.B., Carter, L., Scott, G., Bostock, H., Bowen, M., et al., 2013. Southwest Pacific Ocean response to a warmer world: Insights from marine isotope stage 5e. Paleoceanography 28, 585–598. https://doi.org/10.1002/palo.20052.

Cortese, G., Prebble, J., 2015. A radiolarian-based modern analogue dataset for palaeoenvironmental reconstructions in the southwest Pacific. Mar. Micropaleontol. 118, 34–49. https://doi.org/10.1016/j.marmicro.2015.05.002.

Crosta, X., Kohfeld, K.E., Bostock, H.C., Chadwick, M., Du Vivier, A., Esper, O., Etourneau, J., Jones, J., Leventer, A., Müller, J., Allen, C.S., Ghadi, P., Lamping, N., Lange, C.B., Lund, D., Marzocchi, A., Meissner, K.J., Menviel, L., Nair, A., Patterson, M., Pike, J., Prebble, J.G., Sadatzki, H., Sime, L.C., Shukla, S.K., Thöle, L., Xiao, W., Yang, J., 2022. Antarctic sea ice over the past 130,000 years, Part 1: a review of what proxy records tell us. Clim. Past. https://doi.org/10.5194/cp-18-1729-2022.

Crundwell, M., Scott, G., Naish, T., Carter, L., 2008. Glacial-interglacial ocean climate variability from planktonic foraminifera during the Mid-Pleistocene transition in the temperate Southwest Pacific, ODP Site 1123. Palaeogeogr. Palaeoclimatol. Palaeoecol. 260, 202–229. https://doi.org/10.1016/j.palaeo.2007.08.023.

Davis, R.E., 1998. Preliminary results from directly measuring middepth circulation in the tropical and South Pacific. J. Geophys. Res. Ocean. 103, 24619–24639. https://doi.org/10.1029/98JC01913.

De'Ath, G., 2002. Multivariate regression trees : a new technique for modeling species-environment relationships. Ecology 83, 1105–1117. https://doi.org/10.1890/0012-9658(2002)083[1105:MRTANT]2.0.CO;2.

Ellwood, M.J., Wille, M., Maher, W., 2010. Glacial silicic acid concentrations in the Southern Ocean. Science 330, 1088–1091. https://doi.org/10.1126/science.1194614.

Elmore, A.C., McClymont, E.L., Elderfield, H., Kender, S., Cook, M.R., Leng, M.J., Greaves, M., Misra, S., 2015. Antarctic Intermediate Water properties since 400 ka recorded in infaunal (Uvigerina peregrina) and epifaunal (Planulina wuellerstorfi) benthic foraminifera. Earth Planet Sci. Lett. 428, 193–203. https://doi.org/10.1016/j.epsl.2015.07.013.

Forcén-Vázquez, A., Williams, M.J.M., Bowen, M., Carter, L., Bostock, H.C., 2021. Frontal dynamics and water mass variability on the Campbell Plateau. New Zeal. J. Mar. Freshw. Res. 55, 199–222. https://doi.org/10.1080/00288330.2021.1875490.

Garcia, H.E., Boyer, T.P., Baranoba, R.A., Locarnini, A.V., Mishonov, A., Grodsky, A., Paver, C.R., Weathers, K.W., Smolyar, I.V., Reagan, J.R., Seidov, D., Zweng, M.M., 2019. World Ocean Atlas 2018. NOAA National Centers for Environmental Infomation. Dataset.

Hayward, B.W., Sabaa, A., Grenfell, H.R., 2004. Benthic foraminifera and the late Quaternary (last 150 ka) paleoceanographic and sedimentary history of the Bounty Trough, east of New Zealand. Palaeogeogr. Palaeoclimatol. Palaeoecol. 211, 59–93. https://doi.org/10.1016/j.palaeo.2004.04.007.

Hayward, B.W., Scott, G.H., Crundwell, M.P., Kennett, J.P., Carter, L., Neil, H.L., Sabaa, A.T., Wilson, K., Rodger, J.S., Schaefer, G., Grenfell, H.R., Li, Q., 2008. The effect of submerged plateaux on Pleistocene gyral circulation and sea-surface temperatures in the Southwest Pacific. Glob. Planet. Change 63, 309–316. https://doi.org/10.1016/j.gloplacha.2008.07.003.

Heath, R.A., 1981. Oceanic fronts around southern New Zealand. Deep Sea Res. Part A, Oceanogr. Res. Pap. 28, 547–560. https://doi.org/10.1016/0198-0149(81)90116-3.

Hernández-Almeida, I., Cortese, G., Yu, P.S., Chen, M.T., Kucera, M., 2017. Environmental determinants of radiolarian assemblages in the western Pacific since the last deglaciation. Paleoceanography 32, 830–847. https://doi.org/10.1002/2017PA003159.

Imbrie, J., Kipp, N.G., 1971. A new micropaleontological method for quantitative paleoclimatology: application to a late Pleistocene Caribbean core. In: Turekian, K.K. (Ed.), Late Cenozoic Glacial Ages. Yale University Press, New Haven, CT, pp. 71–181.

Jacot Des Combes, H., Abelmann, A., 2007. A 350-ky radiolarian record off Lüderitz, Namibia-evidence for changes in the upwelling regime. Mar. Micropaleontol. 62, 194–210. https://doi.org/10.1016/j.marmicro.2006.08.004.

Jacot Des Combes, H., Caulet, J.P., Tribovillard, N.P., 1999. Pelagic productivity changes in the equatorial area of the northwest Indian Ocean during the last 400,000 years. Mar. Geol. 158, 27–55. https://doi.org/10.1016/S0025-3227(98)00163-7.

Jacot Des Combes, H., Pierre Caulet, J., Tribovillard, N., 2005. Monitoring the variations of the Socotra upwelling system during the last 250 kyr: a biogenic and geochemical approach. Palaeogeogr. Palaeoclimatol. Palaeoecol. 223, 243–259. https://doi.org/10.1016/j.palaeo.2005.04.007.

Juggins, S., 2013. Quantitative reconstructions in palaeolimnology: new paradigm or sick science? Quat. Sci. Rev. 64, 20–32. https://doi.org/10.1016/j.quascirev.2012.12.014.

Kling, S.A., 1976. Relation of radiolarian distributions to subsurface hydrography in the North Pacific. Deep. Res. Oceanogr. Abstr. 23, 1043–1058. https://doi.org/10.1016/0011-7471(76)90880-9.

Kling, S.A., Boltovskoy, D., 1995. Radiolarian vertical distribution patterns across the Southern California current. Deep. Res. Part I 42. https://doi.org/10.1016/0967-0637(94)00038-T.

Lawler, K., Cortese, G., Civel-Mazens, M., Bostock, H.C., Crosta, X., Leventer, A., Lowe, V., Rogers, J., Armand, L.K., 2021. The Southern Ocean RADiolarian (SO-RAD) dataset: a new compilation of modern radiolarian census data. Earth Syst. Sci. Data Discuss. 1–23. https://doi.org/10.5194/essd-2021-148.

Lazarus, D., 2005. A brief review of radiolarian research. Paläontol. Z. 79, 183–200. https://doi.org/10.1007/bf03021761.

Lazarus, D., Bittniok, B., Diester-Haass, L., Billups, K., Ogawa, Y., Takahashi, K., Meyers, P., 2008. Radiolarian and sedimentologic paleoproductivity proxies in late pleistocene sediments of the benguela upwelling system, ODP site 1084. Mar. Micropaleontol. 68, 223–235. https://doi.org/10.1016/j.marmicro.2008.02.004.

Lazarus, D., Bittniok, B., Diester-Haass, L., Meyers, P., Billups, K., 2006. Comparison of radiolarian and sedimentologic paleoproductivity proxies in the latest Miocene-Recent Benguela Upwelling System. Mar. Micropaleontol. 60, 269–294. https://doi.org/10.1016/j.marmicro.2006.06.003.

Legendre, P., Legendre, L., 2012. Ordination in reduced space. In: Numerical Ecology. Elsevier, Oxford, pp. 425–520. https://doi.org/10.1016/B978-0-444-53868-0.50009-5.

Locarnini, R.A., 1994. Water Masses and Circulation in the Ross Gyre and Environs. Texas A&M University.

Lowe, V., Cortese, G., Lawler, K.-A., Civel-Mazens, M., Bostock, H.C., 2022. Ecoregionalisation of the Southern Ocean using radiolarians. Front. Mar. Sci. 9, 1–16. https://doi.org/10.3389/fmars.2022.829676.

Lüer, V., Cortese, G., Neil, H.L., Hollis, C.J., Willems, H., 2009. Radiolarian-based sea surface temperatures and paleoceanographic changes during the Late Pleistocene-Holocene in the subantarctic southwest Pacific. Mar. Micropaleontol. 70, 151–165. https://doi.org/10.1016/j.marmicro.2008.12.002.

Lüthi, D., Le Floch, M., Bereiter, B., Blunier, T., Barnola, J.M., Siegenthaler, U., Raynaud, D., Jouzel, J., Fischer, H., Kawamura, K., Stocker, T.F., 2008. High-resolution carbon dioxide concentration record 650,000-800,000 years before present. Nature 453, 379–382. https://doi.org/10.1038/nature06949.

Marshall, J., Speer, K., 2012. Closure of the meridional overturning circulation through Southern Ocean upwelling. Nat. Geosci. 5, 171–180. https://doi.org/10.1038/ngeo1391.

Matsuzaki, K.M., Itaki, T., 2017. New northwest Pacific radiolarian data as a tool to estimate past sea surface and intermediate water temperatures. Paleoceanography 32, 218–245. https://doi.org/10.1002/2017PA003087.

Matsuzaki, K.M., Itaki, T., Sugisaki, S., 2020. Polycystine radiolarians vertical distribution in the subtropical Northwest Pacific during Spring 2015 (KS15-4). Paleontol. Res. 24 (2), 1–21. https://doi.org/10.2517/2019PR019.

McCave, I.N., Carter, L., Hall, I.R., 2008. Glacial-interglacial changes in water mass structure and flow in the SW Pacific Ocean. Quat. Sci. Rev. 27, 1886–1908. https://doi.org/10.1016/j.quascirev.2008.07.010.

Neil, H.L., Carter, L., Morris, M.Y., 2004. Thermal isolation of Campbell Plateau, New Zealand, by the antarctic circumpolar current over the past 130 kyr. Paleoceanography 19, 1–17. https://doi.org/10.1029/2003PA000975.

Noble, T.L., Piotrowski, A.M., McCave, I.N., 2013. Neodymium isotopic composition of intermediate and deep waters in the glacial southwest Pacific. Earth Planet Sci. Lett. 384, 27–36. https://doi.org/10.1016/j.epsl.2013.10.010.

Oksanen, J., Blanchet, F.G., Friendly, M., Kindt, R., Legendre, P., Mcglinn, D., Minchin, P. R., O'Hara, R.B., Simpson, G.L., Solymos, P., Stevens, M.H.H., Szoecs, E., Wagner, H., 2019. Vegan: community Ecology package. R package version 2.4-2. Community Ecol. Packag. 2 (5–6), 1–296.

Orsi, A.H., Whitworth, T., Nowlin, W.D., 1995. On the meridional extent and fronts of the Antarctic Circumpolar Current. Deep Sea Res. I Oceanogr. Res. Pap. 42, 641–673. https://doi.org/10.1016/0967-0637(95)00021-W.

Orsi, A.H., Wiederwohl, C.L., 2009. A recount of Ross Sea waters. Deep. Res. Part II Top. Stud. Oceanogr. 56, 778–795. https://doi.org/10.1016/j.dsr2.2008.10.033.

Ouellette, M.-H., Legendre, P., 2014. Package 'MVPARTwrap.

Pahnke, K., Zahn, R., 2005. Southern hemisphere water mass conversion linked with North Atlantic climate variability. Science 307, 1741–1746. https://doi.org/10.1126/science.1102163.

Pahnke, K., Zahn, R., Elderfield, H., Schulz, M., 2003. 340,000-year centennial-scale marine record of Southern Hemisphere climatic oscillation. Science 301, 948–952. https://www.science.org/doi/10.1126/science.1084451.

Panitz, S., Cortese, G., Neil, H.L., Diekmann, B., 2015. A radiolarian-based palaeoclimate history of Core Y9 (Northeast of Campbell Plateau, New Zealand) for the last 160 kyr. Mar. Micropaleontol. 116, 1–14. https://doi.org/10.1016/j.marmicro.2014.12.003.

Pellichero, V., Sallée, J.B., Chapman, C.C., Downes, S.M., 2018. The southern ocean meridional overturning in the sea-ice sector is driven by freshwater fluxes. Nat. Commun. 9, 1–9. https://doi.org/10.1038/s41467-018-04101-2.

Prebble, J.G., Bostock, H.C., Cortese, G., Lorrey, A.M., Hayward, B.W., Calvo, E., Northcote, L.C., Scott, G.H., Neil, H.L., 2017. Evidence for a Holocene climatic optimum in the Southwest Pacific: a multiproxy study. Paleoceanography 32, 763–779. https://doi.org/10.1002/2016PA003065.

Rintoul, S.R., Sokolov, S., Williams, M.J.M., Molino, B.P., Rosenberg, M., Bindoff, N.L., 2014. Antarctic circumpolar current transport and barotropic transition at Macquarie Ridge. Geophys. Res. Lett. 41, 7254–7261. https://doi.org/10.1002/2014GL061880.

Rogers, J., De Deckker, P., 2007. Radiolaria as a reflection of environmental conditions in the eastern and southern sectors of the Indian Ocean: a new statistical approach. Mar. Micropaleontol. 65, 137–162. https://doi.org/10.1016/j.marmicro.2007.07.001.

Ronge, T.A., Steph, S., Tiedemann, R., Prange, M., Merkel, U., Nürnberg, D., Kuhn, G., 2015. Pushing the boundaries: glacial/interglacial variability of intermediate and deep waters in the southwest Pacific over the last 350,000 years. Paleoceanography 30, 23–38. https://doi.org/10.1002/2014PA002727.

Ronge, T.A., Tiedemann, R., Lamy, F., Köhler, P., Alloway, B.V., De Pol-Holz, R., Pahnke, K., Southon, J., Wacker, L., 2016. Radiocarbon constraints on the extent and evolution of the South Pacific glacial carbon pool. Nat. Commun. 7, 1–12. https://doi.org/10.1038/ncomms11487.

Schlitzer, R., 2020. Ocean data View. Available at: https://odv.awi.de.

Sikes, E.L., Samson, C.R., Guilderson, T.P., Howard, W.R., 2000. Old radiocarbon ages in the southwest Pacific Ocean during the last glacial period and deglaciation. Nature 405, 555–559. https://doi.org/10.1038/35014581.

Skinner, L., McCave, I.N., Carter, L., Fallon, S., Scrivner, A.E., Primeau, F., 2015. Reduced ventilation and enhanced magnitude of the deep Pacific carbon pool during the last glacial period. Earth Planet Sci. Lett. 411, 45–52. https://doi.org/10.1016/j.epsl.2014.11.024.

Sokolov, S., Rintoul, S.R., 2007. Multiple jets of the antarctic circumpolar current south of Australia. J. Phys. Oceanogr. 37 (1), 1394–1412. https://doi.org/10.1175/JPO3111.

Sokolov, S., Rintoul, S.R., 2009. Circumpolar structure and distribution of the antarctic circumpolar current fronts: 1. Mean circumpolar paths. J. Geophys. Res. Ocean. 114, 1–19. https://doi.org/10.1029/2008JC005108.

Stepanjants, S., Cortese, G., Kruglikova, S., Bjørklund, K., 2006. A review of bipolarity concepts: history and examples from Radiolaria and Medusozoa (Cnidaria). Mar. Biol. Res. 2, 200–241. https://doi.org/10.1080/17451000600781767.

Stickley, C.E., Brinkhuis, H., Schellenberg, S.A., Sluijs, A., Röhl, U., Fuller, M., Grauert, M., Huber, M., Warnaar, J., Williams, G.L., 2004. Timing and nature of the deepening of the tasmanian gateway. Paleoceanography 19, 1–18. https://doi.org/10.1029/2004PA001022.

Sutton, P.J.H., 2003. The Southland current: a subantarctic current. New zeal. J. Mar. Freshw. Res. 37, 645–652. https://doi.org/10.1080/00288330.2003.9517195.

Tapia, R., Nürnberg, D., Ho, S.L., Lamy, F., Ullermann, J., Gersonde, R., Tiedemann, R., 2019. Glacial differences of Southern Ocean intermediate waters in the central South Pacific. Quat. Sci. Rev. 208, 105–117. https://doi.org/10.1016/j.quascirev.2019.01.016.

Therneau, T.M., 2022. mvpart: Mulitvariate partitioning. R package version 1.6-3. https://github.com/richardjtelford/mvpart.

Welling, L.A., 1997. Environmental Control of Radiolarian Abundance in the Central Equatorial Pacific and Implications for Paleoceanographic Reconstructions. Ph.D. Thesis. Oregon State University, Oregon, USA.

Wells, P., Okada, H., 1997. Response of nannoplankton to major changes in sea-surface temperature and movements of hydrological fronts over Site DSDP 594 (south Chatham Rise, southeastern New Zealand), during the last 130 kyr. Mar. Micropaleontol. 32, 341–363. https://doi.org/10.1016/S0377-8398(97)00025-X.

Wickham, H., 2016. ggplot2: Elegant Graphics for Data Analysis.

Wilson, K., Hayward, B.W., Sabaa, A.T., Scott, G.H., Kennett, J.P., 2005. A one-million-year history of a north-south segment of the Subtropical Front, east of New Zealand. Paleoceanography 20, 1–10. https://doi.org/10.1029/2004PA001080.

Yamashita, H., Takahashi, K., Fujitani, N., 2002. Zonal and vertical distribution of radiolarians in the western and central Equatorial Pacific in January 1999. Deep-Sea Res. 49, 2823–2862.

Zoccarato, L., Pallavicini, A., Cerino, F., Fonda Umani, S., Celussi, M., 2016. Water mass dynamics shape Ross Sea protist communities in mesopelagic and bathypelagic layers. Prog. Oceanogr. 149, 16–26. https://doi.org/10.1016/j.pocean.2016.10.003.